Thermal-conductivity measurements in liquid ^{4}He below 0.7 K

Dennis S. Greywall
Bell Laboratories, Murray Hill, New Jersey 07974
(Received 9 October 1980)

High-precision steady-state heat-flow measurements were made in pure liquid ^{4}He under pressures of up to 25 bar. The data cover the temperature range between 0.1 and 0.7 K and were obtained using sample containment tubes which ranged in diameter from 0.14 to 1.4 cm. The data yield information about Λ, the phonon mean free path for large-angle scattering. At the higher pressures phonon-roton scattering plays a significant role in limiting Λ. However, at low pressures and temperatures the Λ results show evidence that three-phonon processes become dominant. This permits inferences to be made concerning the phonon dispersion relation. In the temperature regime for which Λ is comparable with the tube diameter, a phenomenon was observed which is analogous to the Knudsen minimum observed in ordinary-gas flow measurements. These data are compared with the recent calculations of Benin and Maris.

I. INTRODUCTION

At very low temperatures the thermal excitations in liquid ^{4}He, i.e., the long-wavelength phonons, travel ballistically and scatter only from the walls of the container. This is the process which restricts the flow of heat and so in general the effective thermal conductivity at low temperature must depend on the size and shape of the container and also on the smoothness of the surface. For the special case of an infinitely-long cylindrical container with walls which scatter the phonons diffusively, Casimir[1] showed that the conductivity is given by

$$\kappa_{\text{Casimir}} = \tfrac{1}{3} C_{ph} \langle c_g \rangle d \quad , \tag{1}$$

where C_{ph} is the phonon specific heat per unit volume, $\langle c_g \rangle$ is the average group velocity of the phonons, and d is the tube diameter. The effective mean free path of the phonons is thus, in this case, precisely equal to d.

With increasing temperature the phonon density increases and Λ becomes limited by phonon-phonon interactions. In the regime where $\Lambda \ll d$, the phonons in superfluid ^{4}He can be treated as a gas of particles with viscosity η which is driven through the tube via the gradient in fountain pressure set up by the gradient in temperature. It then follows using Poiseuille's formula for the volume flow rate of the gas and the expression

$$\eta = \tfrac{1}{5} \rho_n \langle c_g \rangle \Lambda \tag{2}$$

that

$$\kappa = \tfrac{5}{32} \frac{d}{\Lambda} g \kappa_{\text{Casimir}} \quad , \tag{3}$$

with

$$g \equiv \frac{3 S_{ph}^2 T}{\rho_n \langle c_g \rangle^2 C_{ph}} \quad . \tag{4}$$

The quantity g is approximately equal to unity. In this viscous flow regime, which was first experimentally observed by Whitworth,[2] the conductivity thus increases with a temperature dependence which is greater than the T^3 dependence characteristic of the boundary scattering regime.

When $\Lambda \approx d$, Whitworth found that the thermal conductivity increases slower than T^3. This result is similar to the Knudsen minimum observed in ordinary-gas flow measurements. Simons[3] and more recently Benin and Maris[4] have theoretically studied this intermediate regime and have been able to show from their very different Boltzman equation approaches that such a minimum should occur. A simple physical explanation of the minimum has however not been given.

In this paper we report liquid ^{4}He thermal conductivity results obtained using five different sample tubes which ranged in diameter from 0.14 to 1.4 cm. These tube diameters are such that the measurements in the temperature range from 0.1 to 0.7 K include the regime where $\Lambda \approx d$ and thus show the transition from Casimir to viscous flow behavior. This experiment is thus similar to that performed by Whitworth,[2] however the experimental techniques have been improved considerably leading to more quantitative results. In addition, the temperature range has been extended to lower temperatures and measurements have now been made under pressure.

In Sec. II we give the experimental details. The conductivity data are presented in Sec. III followed by

a discussion of various complicating factors such as the possible specular reflection of the phonons at the tube walls, the effects of using a sample tube of finite length, the slip of the normal fluid at the boundary, and the effects due to the presence of the rotons. We then give the results for Λ obtained from the data in the viscous flow regime. Implications about the phonon dispersion relation are discussed. The transition region is then considered.

II. EXPERIMENTAL DETAILS

A. Apparatus

A diagram of the experimental apparatus used to measure the thermal conductivity is shown in Fig. 1. It consisted of five vertical sample tubes joined together at their lower ends via a circular copper manifold which was in good thermal contact with the mixing chamber of a dilution refrigerator. The nickel tubes ranged in diameter from 0.14 to 1.4 cm and had length-to-diameter ratios of about 20, see Table I. The wall thickness was 1% of the tube diameter. Each of the tubes was closed at its upper end with a copper cap. Heaters, with superconducting leads, wound on the outside of each of these caps were used to measure the thermal conductance of the empty tubes. To avoid problems associated with the thermal boundary resistance, other heaters suspended inside the caps were used when the apparatus was filled with liquid helium. Two close-fitting copper tabs made from 0.8-mm-thick copper sheet were soft soldered to each tube. These thermometer supports were positioned nominally 10 tube diameters apart. Carbon thermometers and metal film reference resistors were varnished onto these tabs.

The helium samples were confined to constant volume using a valve[5] which was mounted on the manifold. Also located on the manifold were a heater and thermometer for temperature control; a germanium thermometer which had been calibrated[6] against the ^{3}He vapor pressure scale in the range from 0.3 to 1 K; and a cerium magnesium nitrate (CMN) thermometer.[7]

In order to reduce the amount of specular reflection of the phonons from the container walls, each of the sample tubes was fabricatred by electroplating nickel onto an aluminum mandrel whose outside surface had first been sand blasted using fine glass beads. Thus after the leaching away of the mandrels, the nickel tubes were left with "rough" inside surfaces. An electron microscope picture of the surface is shown in Fig. 2. It was hoped that the roughness created in this manner would be uniform over the whole surface and the same for each of the tubes (see Sec. III D).

TABLE I. Sample tube parameters measured at room temperature. The thermometer spacing was measured between the midpoints of the copper tabs soldered to the nickel tubes. The wall thickness of each of the tubes was 1% of the diameter.

Tube No.	Diameter (cm)	Thermometer spacing (cm)	Tube length (cm)
1	0.138	1.43	3.6
2	0.232	2.50	5.5
3	0.474	4.61	10.4
4	0.797	8.40	15.6
5	1.427	15.19	25.4

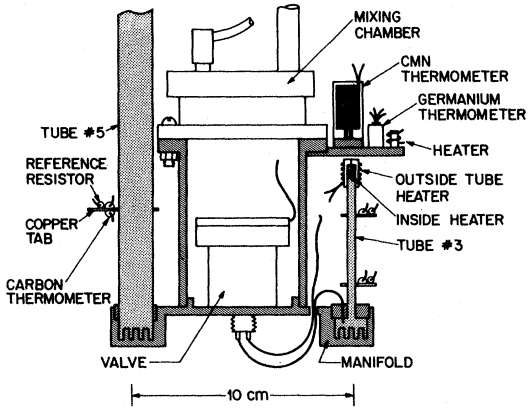

FIG. 1. Thermal conductivity apparatus.

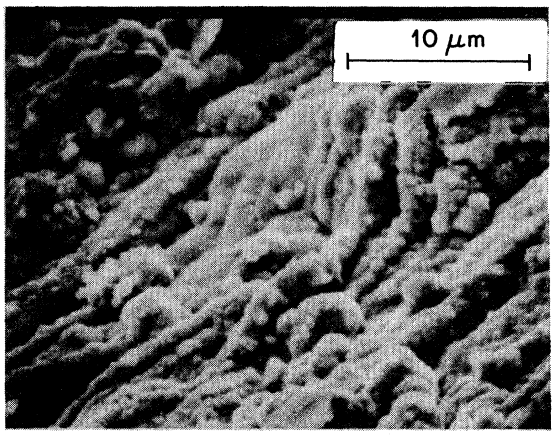

FIG. 2. Inside surface of the sample containment tubes.

B. Thermometry

The temperature was measured at the positions of the two copper tabs on each of the tubes, see Fig. 1, using 470 Ω, 0.5 W Speer carbon resistors. They were ground flat on one side and varnished down with cigaretter paper insulation onto the tabs alongside 10 kΩ metal film resistors. The latter resistors showed very little temperature dependence below 1 K and were used as reference resistors. In addition, differential thermometers were used on the two largest tubes. These thermometers each consisted of a well-matched pair of Speer resistors: one mounted on the upper tab, the second on the lower tab. Each of the ten thermometer-and-reference-resistor pairs, as well as the differential thermometer pairs, could be switched into either of two ac resistance bridges.[8]

These resistance thermometers were calibrated against a CMN thermometer,[7] which had in turn been indirectly calibrated (between 0.36 and 1 K) against a high-precision, *in situ*, ^{3}He vapor pressure gauge.[6] The calibrations were made during the actual course of the data taking and were repeated each time the thermometers were used (see Sec. II C).

For temperatures below a few tenths K, Anderson *et al.*[9] have demonstrated that the temperature dependence of Speer carbon resistors is well described by the function

$$R = R_0 \exp(AT^{-1/4}) \ . \tag{5}$$

We have found that by adding a temperature-independent series resistance term to Eq. (5), the range over which our calibration data could be well fitted was extended considerably. Using the expression

$$R = R_S + R_0 \exp(AT^{-1/4}) \ , \tag{6}$$

with R_S, R_0, and A as adjustable parameters, the rms deviation of the temperature was typically 0.3% for fits covering the temperature range from 50 mK to 0.7 K. We note that over this range the resistance changes by more than two orders of magnitude (see Fig. 3). However, since an even better fit of the calibration data was required it was necessary to add more adjustable parameters. This was done by rewriting Eq. (6) with $T^{-1/4}$ as the dependent variable and adding terms proportional to higher powers of $\ln(R - R_S)$, i.e., in our final analysis we used the fitting function

$$T^{-1/4} = \sum_{i=0}^{5} a_i [\ln(R - R_S)]^i \ , \tag{7}$$

with the a_i adjustable and R_S set equal to 1250 Ω for all of the thermometers. It is possible that fewer terms would be needed if the bridge reference resistances were truly temperature independent and if the self-heating in the thermometers was reduced.

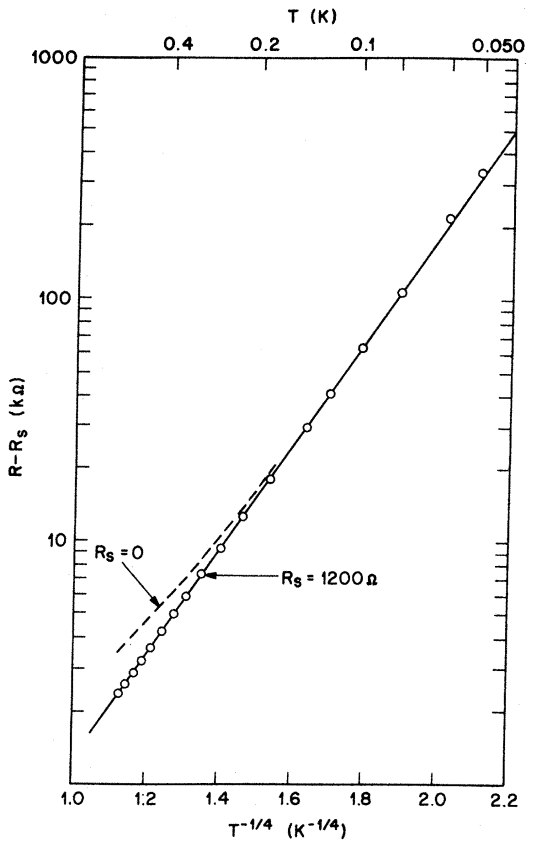

FIG. 3. Calibration data for a thermometer made from a 470 Ω Speer resistor. The straight line corresponds to the relation $\ln(R - R_S) = AT^{-1/4}$ with $R_S = 1200$ Ω.

The bridges were driven at an rms excitation level of 0.7 mV when the thermometer-reference resistor pairs were used. This corresponded to a resolution in the bridge ratio-transformer reading, $\mathfrak{R} = R/(R + R_{\text{ref}})$, of about 10^{-5} and implied a relative temperature resolution $\delta T/T$ of at least 10^{-4} for temperatures in the range from 0.1 to 0.7 K. Thus using these thermometers a temperature difference ΔT between a pair of tabs equal to $0.05T$ could potentially be measured to a precision of at least 0.2%. However, due to the very large thermal conductance of the largest filled tubes at the higher temperatures, it was sometimes impossible to generate a ΔT of this magnitude without exceeding the cooling power of the refrigerator. It was thus necessary to measure much smaller ΔT's with high precision. This was possible using the differential thermometers since these bridges could be driven with higher excitation voltages (see Sec. II C).

The calibration of the differential thermometers was based on the fact that all of the 470 Ω Speer resistors tested had a very similar temperature dependence. The similarity of the particular pairs of resis-

tors in the differential thermometers was directly demonstrated by the fact that with no heat flowing through the conductivity tubes ($\dot{Q}=0$) the ratio transformer reading, $\mathcal{R}_{d,0}=R_{d,t}(T_0)/[R_{d,t}(T_0)+R_{d,b}(T_0)]$ was near 0.5 and varied little with temperature. $R_{d,t}$ and $R_{d,b}$ are the resistances of the resistors in the differential bridge circuit on the top and bottom tabs, respectively. With the constraint that the lower tab temperature, T_b, be maintained constant at T_0, the differential bridge ratio $\mathcal{R}_d$ with $\dot{Q}\neq 0$ is related to $\mathcal{R}_{d,0}$ via the expression

$$z \equiv \frac{\mathcal{R}_d}{1-\mathcal{R}_d}\Big/\frac{\mathcal{R}_{d,0}}{1-\mathcal{R}_{d,0}} = \frac{R_{d,t}(T_t)}{R_{d,t}(T_b)} \quad . \tag{8}$$

If it is assumed that over the complete temperature range the resistance-temperature relation can be expressed in the form $R=R_0\exp(AT^{-\gamma})$ where $\gamma(\neq\frac{1}{4})$ is the same for each of the carbon thermometers, then it follows that for small temperature differences

$$\frac{R_{d,t}(T_t)}{R_{d,t}(T_b)} = \frac{R_b(T_t)}{R_b(T_b)}\left[1+\frac{A_{d,t}-A_b}{A_{d,t}}(z-1)\right] \quad , \tag{9}$$

where R_b corresponds to the resistor in the regular bridge circuit on the lower tab. Thus the temperature of the upper tab can be computed using the relation

$$R_b(T_t)=R_b(T_b)z\left[1-\frac{\delta A}{A}(z-1)\right] \tag{10}$$

and the calibration of R_b which was discussed above. The quantity $\delta A/A$ was determined by comparing low-temperature ($T\lesssim 0.35$ K) thermal conductivity data obtained using the regular bridge thermometers with data obtained using the differential thermometer but analyzed for various choices of $\delta A/A$. For tubes 4 and 5 we found respective values of 0.03 and 0.05. We note that the conductivity values resulting from using $\delta A/A=0.05$ differed from those obtained with $\delta A/A=0$ by a relative amount which varied little with temperature and was roughly 5% at 0.3 K.

The power dissipated in the thermometers and reference resistors was always insignificant compared to the power supplied to the tube heater.

C. Procedure

Because of the large number of leads required for each conductivity tube, it was possible, without serious modification to the cryostat, to make simultaneous electrical connections to at most three tubes. Therefore the data had to be obtained on two cooldowns of the apparatus. Prior to cooling, the cell (Fig. 1) was evacuated using a copper tube soldered into the manifold. This tube was then crimped and soldered closed.

The thermal conductivity measurements were made using the conventional technique: A known quantity of heat $\dot{Q}$ was forced to flow through the sample by dissipating power in the resistor located very near the top of the sample. The resulting equilibrium temperature difference ΔT between two points in the sample was then measured and related to the thermal conductivity κ at the mean temperature via the expression

$$\dot{Q}=\kappa A\,\Delta T/\Delta x \quad . \tag{11}$$

Here A is the uniform cross-sectional area of the sample, and Δx is the spacing between the thermometers. We note that using this simple expression, which determines an average conductivity, introduces a relative error which is approximately equal[10] to $\frac{1}{4}(\Delta T/T)^2$. This quantity was less than 0.1% for all of our measurements and no correction was applied to the results.

After making some very preliminary measurements of the conductance of each of the empty tubes, the final data for each empty tube was obtained according to the following procedure. First, the cell was regulated at 80 mK using the germanium thermometer and heater mounted on the manifold. The bridge ratios of the two tube thermometers were then recorded along with the resistance of the germanium thermometer and the bridge ratio of the CMN thermometer. Once this thermometer calibration data was obtained, power was dissipated in the outside heater (see Sec. II A) at a level estimated, from the preliminary measurements, to result in a temperature difference between the two tube thermometers equal to 6% of the temperature. The heater current was accurately determined using a potentiometer to measure the voltage drop across a standard resistor. After equilibrium had been reestablished, with the manifold being regulated at its initial temperature, the new resistance bridge ratios and the heater current were recorded. The temperature was then increased in steps of 20 mK and the procedure repeated. Typically 20 min were required to obtain the seven quantities corresponding to each "datum point."

After these measurements were completed, helium (0.002 4-ppm ^{3}He) was admitted to the cell and measurements were made on filled tubes at nominal cell pressures of 0, 2, 5, 10, 15, 20, and 25 bar. The helium samples were confined to constant volume by closing the cold valve at 0.1 K (see Fig. 1).

The data taking procedure followed for the three smallest filled tubes differed slightly from that described above. Because of the large thermal conductance of the helium samples it was possible to use the thermometer on the lower tab of the tube being studied in the temperature control loop. Thus when the inside heater at the top of the tube was turned on, the mixing chamber and manifold temperature

decreased so that after equilibrium was reestablished the temperature at the position of the lower tab was unchanged from its initial reading. Because of the greater sensitivity of the bridge thermometer it was possible to regulate the temperature with higher precision. This method also facilitated achieving the desired temperature difference between the upper and lower tabs at any given temperature. Using tables based on preliminary calibrations of each of the tube thermometers, the heater current could be easily adjusted to give a $\Delta T/T$ of roughly 0.06. This was however contingent upon the dilution refrigerator having sufficient cooling power. In Fig. 4 the heater power necessary to generate a ΔT of $\sim 0.06T$, is plotted for each of the tubes with a sample pressure near zero bar. Also plotted in the approximate cooling power of the refrigerator. The intersection of these curves gives the temperature above which our precision, using the data taking method described above, is necessarily degraded due to insufficient cooling power.

Figure 4 demonstrates that it was necessary to employ an alternate method for the two largest tubes in order to obtain data of meaningful precision at the higher temperatures considered. It was not possible to simply increase the thermometer resolution at the higher temperatures by using a larger bridge excitation voltage since we were also limited by the precision with which the temperature could be regulated. To at least partially circumvent this limitation a differential thermometer was used on the two largest tubes (see Sec. II B). For a fixed heat flow through the tube, a change in the manifold temperature caused a shift δT_b in the temperature of the lower tab and a shift in the upper tab temperature of approximately $(1-3\Delta T/T_b)\delta T_b$. Thus the relative change in the temperature difference measured by the differential thermometer was $3\delta T_b/T_b$. Since the temperature fluctuations were on the order of $10^{-4}T$, ΔT potentially could be measured with a precision of better than 0.1%. However the actual precision of the data obtained using the differential thermometers was in general less than this limiting value. Even when the ΔT's were made as large as the refrigerator would tolerate it was not always possible, because of excessive self-heating in the thermometers, to use a bridge excitation voltage large enough to give the desired temperature resolution. The actual precision achieved is discussed in Sec. II C.

The thermal conductivity results for *each* of the helium samples were extracted from the raw data in the following manner. First, the CMN thermometer calibration was determined using the readings of the germanium thermometer in the temperature range from 0.3 to 0.7 K. Next, the resistance bridge ratios were calibrated against the CMN thermometer, using the ratios recorded with no heat flowing in the tube. These calibration data were fitted with the function discussed in Sec. II B. It was then possible to compute the total thermal conductance of the tube using the measurements made with the heater on. After subtracting off the very small empty-tube conductance, the conductivity of the helium sample was obtained by dividing by the cross sectional area.

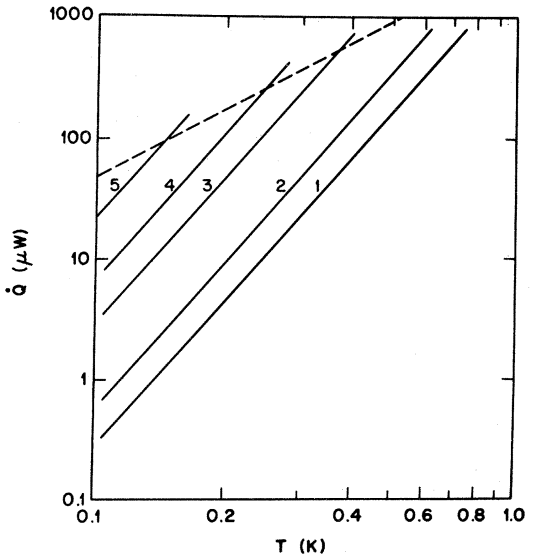

FIG. 4. Approximate power needed to generate a temperature difference between the thermometer tabs of $0.06T$ for each of the five tubes. $P=0.1$ bar. The dashed line shows the cooling power of the refrigerator.

D. Uncertainties in the data

The tube diameters and the spacings between the pairs of thermometer tabs were both known to about 0.5%, while the accuracy of the power dissipation measurements was better than 0.1%. Thus the contribution to the overall uncertainty of the thermal conductivity measurements from these sources of systematic error is roughly 1.5%.

The relative precision with which the temperature-difference measurements could be made was dependent upon: (i) the temperature resolution of the thermometers; (ii) the size of the temperature gradient that it was possible to generate without overloading the refrigerator; and (iii) the precision with which the manifold temperature could be regulated. For the two smallest tubes it was possible to generate a temperature difference of about $0.06T$ for all temperatures and the precision of these data is on the order of a few tenths percent. For tubes 3, 4, and 5 a temperature was reached, beyond which the size of $\Delta T/T$ had to be gradually reduced. As a consequence, the precision of the data for these tubes is reduced at the higher temperatures.

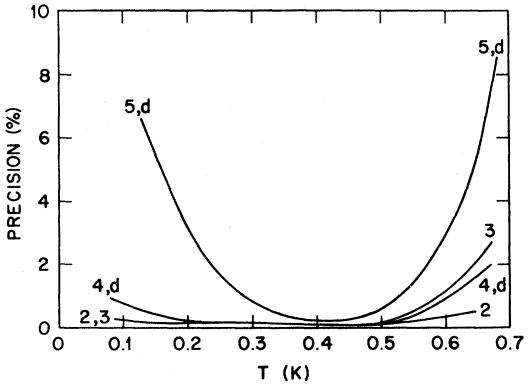

FIG. 5. The relative precision of the thermal conductivity data at $P = 0.1$ bar. The numbers are the tube identification numbers. The suffix d indicates that differential thermometers were used on the two largest tubes.

Figure 5 gives a summary of the estimated precision of the data for each of the five tubes for a sample pressure of 0.1 bar. The suffix d indicates that differential thermometers (Sec. II B) were used for tubes 4 and 5. The reduced precision at the low-temperature end is due partially to the loss of bridge sensitivity associated with the very large resistance of the carbon thermometers at these temperatures. For tube 5, however, a much more significant problem, which may possibly be attributable to experimental difficulties, was the fluctuation of the tab temperatures. The fluctuations were present with and without a heat flow in the tube and increased in relative amplitude with decreasing temperature. A similar, but very much smaller effect was also observed for tube 4.

III. RESULTS AND DISCUSSION

A. Thermal conductivity data

The thermal conductivity results obtained using tubes 1 and 4 (see Table I) and at nominal sample pressures of 2 and 20 bar are shown as a function of temperature on log-log scales in Fig. 6. At sufficiently low temperature, the results should be described by the Casimir relation Eq. (1) which gives the conductivity in the boundary scattering regime ($\Lambda >> d$). In agreement with this expression, the lower temperature data shown in the figure at both pressures closely scale with the tube diameters. The conductivity also decreases with increasing pressure which is consistent with the known decrease in the specific heat. In addition, the data below roughly 0.4 K very nearly fall on straight lines with slopes only slightly less than 3, correspond to the T^3 dependence of the

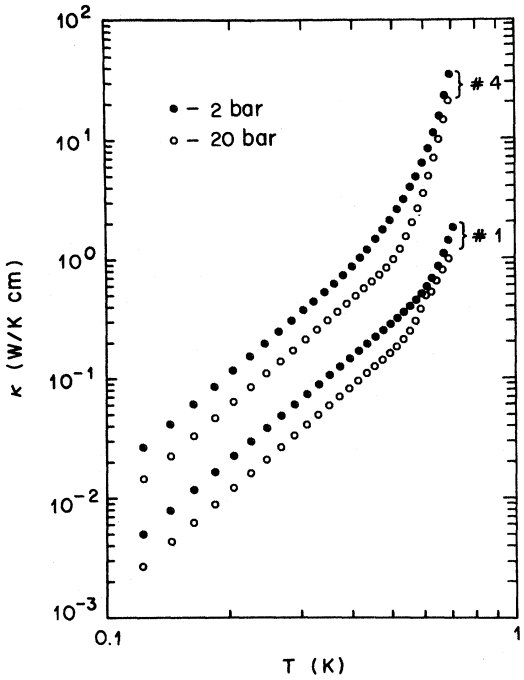

FIG. 6. Thermal conductivity results for tubes 1 and 4 obtained at pressures of 2 and 20 bar.

Debye specific heat. At the higher temperatures the conductivity increases much more rapidly due to the viscous flow of the phonons and to the contribution of the rotons. The transition to the viscous flow regime should occur at some fixed value of Λ/d which means that the deviation from the approximately T^3 behavior should set in at a lower temperature for the larger tube. The data obtained at a sample pressure of 2 bar clearly show this effect. The 20-bar data at the higher temperatures are more complicated partially due to the significant roton contribution to the conductivity. In addition, the 20-bar data for the smaller tube show an abrupt shift and change of behavior near 0.6 K. This occurs near the temperature at which the expansion coefficient becomes negative[11] and the sample becomes unstable when heated from the top. The data obtained with the larger tube to not show this same phenonmenon but the imposed temperature gradients were considerably smaller and apparently not sufficiently large to drive the mechanical flow.

It is convenient to continue the discussion of the thermal conductivity results in terms of the quantity

$$y \equiv \kappa/\kappa_{\text{Casimir}} \ . \tag{12}$$

However, for quantitative results to be obtained, the Casimir expression [Eq. (1)] must be evaluated with account being made for the nonlinear dispersion of the phonons. Even at very low temperatures, the actual phonon specific heat shows significant departures

from the T^3 Debye behavior, but high-precision data[7] for C_{ph} exist and can be directly utilized. The determination of the temperature-dependent phonon group velocity is more involved.

B. Phonon dispersion relation and the average phonon velocity

The average phonon velocity can be computed quite directly if the long-wavelength region of the phonon dispersion relation is known. Since neutron scattering experiments cannot accurately probe this region of the spectrum, quantitative information must be inferred from less direct measurements. In the analysis of the specific-heat data discussed in Ref. 7, the coefficients in a power series in the temperature, which accurately describes the phonon contribution to the measured specific heat, were related directly to the coefficients of an expansion of the phonon energy in powers of the momentum. Very recently, however, Donnelly *et al.*[12] have demonstrated, using the $P=0$ bar data, that this method gives the correct $\epsilon - k$ relation only for the smallest values of k. In this section an outline is given of the method we used to determine the pressure dependent spectrum out to approximately 0.5 Å^{-1}. It is consistent with the specific-heat,[7] neutron scattering,[13] and sound propagation results.[14]

We chose to write the dispersion relation in the form

$$\epsilon = c_0 \hbar k [1 - \alpha_2(P)k^2 - \alpha_4(P)k^4 - \alpha_6(P)k^6] \qquad (13)$$

and imposed the two constraints that at $k = 0.4$ Å^{-1} and at $k = 0.5$ Å^{-1} the spectrum agree with the smoothed neutron results.[13] Equation (13) could thus be rewritten in terms of only one parameter, e.g., α_2. At $P=0$, α_2 was adjusted to give a least-squares fit of the specific-heat data. The computed phonon specific-heat values which were compared with the data in the fitting routine, were determined by numerically evaluating the expression

$$C_{ph} = \frac{V}{2\pi^2 k_B T^2} \int_0^{k_{\max}} \frac{\epsilon^2 e^{\epsilon/k_B T}}{(e^{\epsilon/k_B T} - 1)^2} k^2 dk \quad , \qquad (14)$$

with the integration cutoff at $k_{\max} = 0.5$ Å^{-1}. For the low-temperature data ($T \lesssim 0.7$ K) this cutoff is above the momentum region where a significant contribution is made to the phonon specific heat. The data used were the smoothed results generated using the best-fit expressions for C_{ph} presented in Ref. 7(E). The data were terminated at a temperature beyond which the roton contribution to the total specific heat is larger than 20%. This was done in order to minimize the effects of possible errors in C_{ph} associated with the separation of the total specific heat into phonon and roton terms. The $k=0$ phonon velocity, c_0, was computed directly from the coefficient of the T^3 term given for C_{ph}.[7(b)] The results for α_2 are, of course, quite sensitive to the constraint values used for ϵ at $k = 0.4$ and 0.5 Å^{-1}. This is especially true at the higher pressures. Thus rather than fitting the specific-heat results for $P > 0$, the assumption was made, consistent with the findings presented in Ref. 7, that α_2 depends linearly on the pressure. The further assumption was made that at 20 bar, α_2 is equal to zero which is in general agreement with the results of sound propagation studies.[14] We thus find that the pressure dependences of the parameters of Eq. (13) are given by

$$\alpha_2 = -1.30 + 0.065P \quad ,$$

$$\alpha_4 = -10.25\alpha_2 - 108.5\left(\frac{c_{0.4}}{c_0} - 1\right) + 28.44\left(\frac{c_{0.5}}{c_0} - 1\right) \quad ,$$

$$\alpha_6 = 25.0\alpha_2 + 434.0\left(\frac{c_{0.4}}{c_0} - 1\right) - 177.8\left(\frac{c_{0.5}}{c_0} - 1\right) \quad , \qquad (15)$$

with

$$c_{0.4} \equiv \left.\frac{\epsilon}{\hbar k}\right|_{k=0.4} = 247.0 + 2.86P \quad ,$$

$$c_{0.5} \equiv \left.\frac{\epsilon}{\hbar k}\right|_{k=0.5} = 242.0 + 2.20P \quad .$$

The rms derivation of the phonon specific heat computed using these parameters is about 1% for all pressures. A comparison with the small-k neutron results is given in Fig. 7, which shows the excellent agreement with these data as well.

The isobaric, energy-weighted average group velocity of the phonons was computed as a function of temperature using the expression

$$\langle c_g \rangle = \int_0^{k_{\max}} \frac{\frac{\epsilon}{\hbar}\left(\frac{\partial \epsilon}{\partial k}\right)_P k^2 dk}{e^{\epsilon/k_B T} - 1} \Big/ \int_0^{k_{\max}} \frac{\epsilon k^2 dk}{e^{\epsilon/k_B T} - 1} \quad . \qquad (16)$$

Figure 8 shows that even for temperatures as high as 0.7 K, $\langle c_g \rangle$ differs from c_0 by at most a few percent and thus its use in Eq. (12) has only a small effect on the reduced thermal conductivity y even at the lower pressures.

In Fig. 9 the quantity g, which is defined by Eq. (4) and which will be used later in the analysis, is plotted versus temperature for several pressures. As stated in the Introduction, g departs little from unity.

C. Reduced conductivity y

The experimental data can now be presented in terms of the quantity y defined by Eq. (12). Plotting

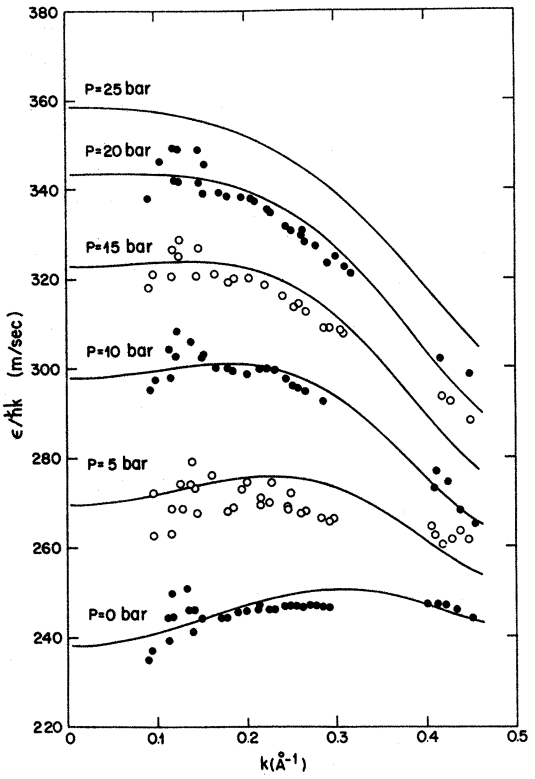

FIG. 7. The phonon dispersion relation extracted from specific-heat measurements [Eqs. (13) and (15)]. Comparison is made with the neutron scattering data of Stirling *et al.* (Ref. 13).

the conductivity in this manner, however, introduces additional errors due to the uncertainties in each of the quantities C_{ph}, $\langle c_g \rangle$, and d which can be exaggerated by uncertainties in the measured sample pressure. The total of these errors is estimated to be of the order of a few percent but should be mainly systematic and thus lead essentially only to an overall shift in y. All of the results with $y < 1.4$ are shown in Fig. 10. The five columns correspond to the measurements made on each of the five sample tubes. Data obtained at the same sample pressure are in rows.

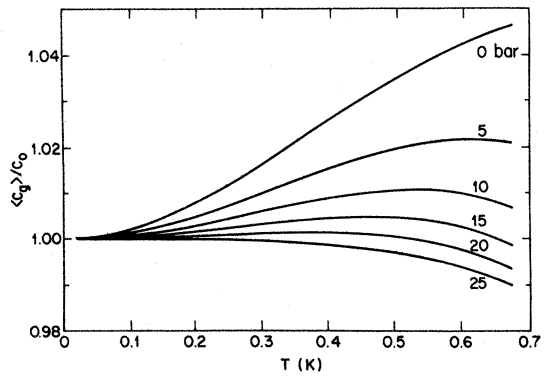

FIG. 8. Temperature dependence of the average phonon group velocity along several isobars.

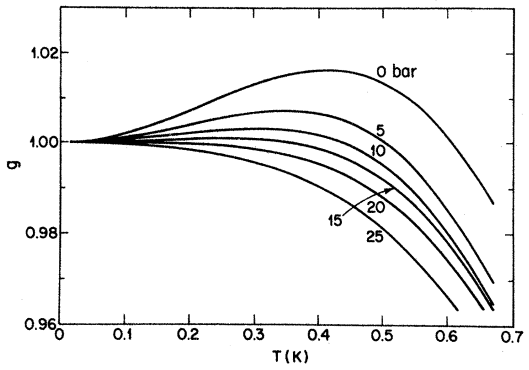

FIG. 9. Temperature dependence of the quantity g defined by Eq. (4) along several isobars.

With the exception of the results for tube 3 each of the strings of data, as expected, tends approximately to one as $T \rightarrow 0$. At the lowest pressure, y exhibits the minimum first seen by Whitworth. However, we now find that this minimum, although shifted in temperature, exists at all pressures up to the melting curve.

The results for tube 3 are obviously inconsistent with the data obtained for the other tubes. As shown below this can be explained if a significant fraction f of the phonons is specularly reflected from the walls of this particular tube. Berman, Simon, and Ziman[15] have shown that for this situation the Casimir expression should be written

$$\kappa_{\text{Casimir}} = \tfrac{1}{3} C_{ph} \langle c_g \rangle d \left(\frac{1+f}{1-f} \right) , \tag{17}$$

which implies then that for tube 3 approximately 10% of the phonons were specularly reflected at 0.1 K.

D. Specular reflection

The fraction of radiation with wavelength λ which is specularly reflected from a uniformly rough surface, characterized by a length scale β, was deduced by Berman, Foster, and Ziman to be given by

$$f_{\text{spec}}(\beta, \lambda) = e^{-8\pi^2\beta^2/\lambda^2} = e^{-2\beta^2 k^2} . \tag{18}$$

Thus for wavelengths large compared to β the surface appears smooth and the radiation is specularly reflected; while for small values of λ, the surface appears rough and the scattering is diffusive. For the

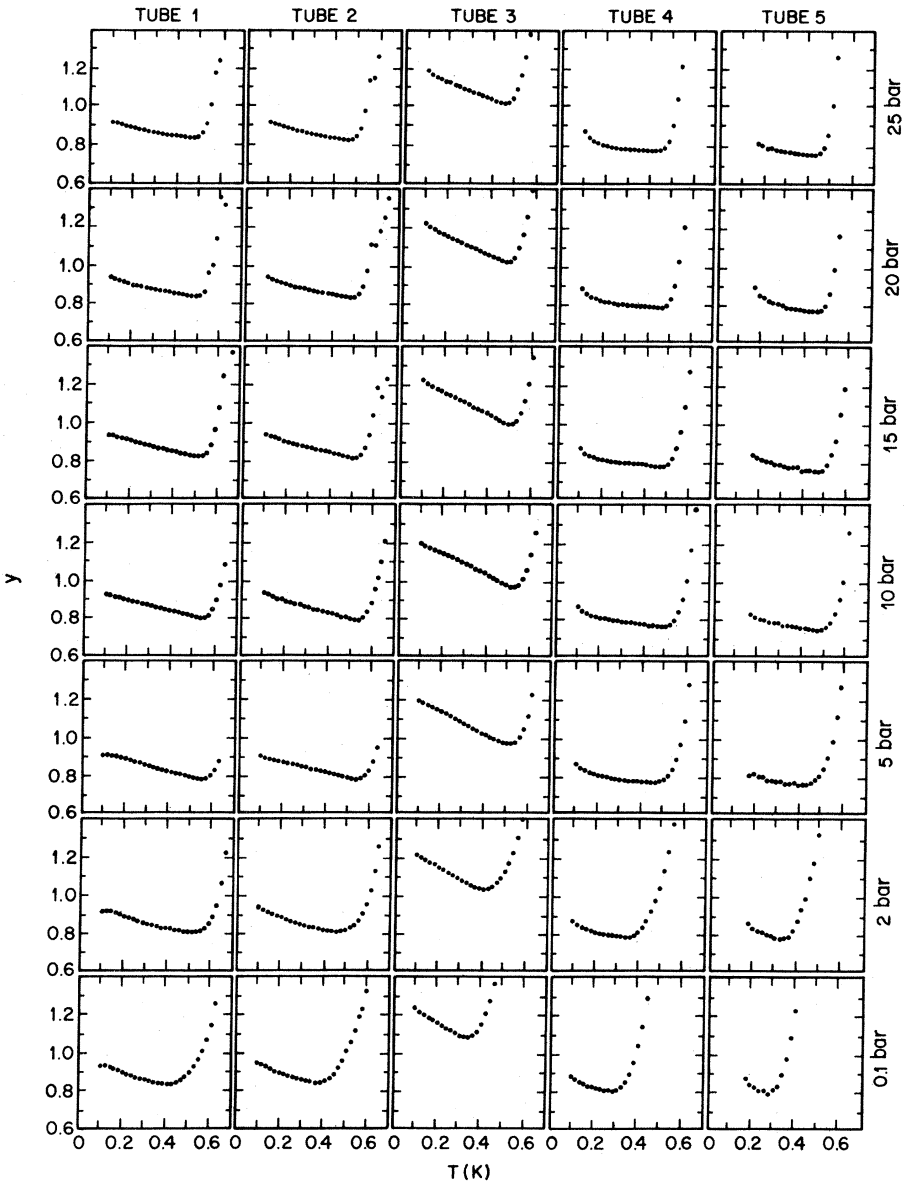

FIG. 10. Reduced thermal conductivity $y \equiv \kappa/\kappa_{\text{Casimir}}$ vs temperature.

case of phonons the situation is more complicated since there is a temperature-dependent distribution of wavelengths. Here the fraction of energy flux (at low temperatures) which is specularly reflected is computed by evaluating the expression

$$f \equiv f_{\text{spec}}(\beta, T) = \int_0^\infty \frac{e^{-2\beta^2 k^2} \epsilon k^2 dk}{e^{\epsilon/k_B T} - 1} \Big/ \int_0^\infty \frac{\epsilon k^2 dk}{e^{\epsilon/k_B T} - 1} . \tag{19}$$

Results of f vs T at $P = 0$ bar, obtained by numerical integration, are plotted for several values of β in Fig. 11(a). In Fig. 11(b) the quantity $(1+f)/(1-f)$ which appears in Eq. (17), the modified form of Casimir's relation, is plotted as a function of temperature. Note that at sufficiently low temperature the fraction of phonons specularly reflected will always become large since the wavelengths of the dominant phonons progressively increase with decreasing temperature. This is shown explicitly in Fig. 12 where the integrand of the denominator of Eq. (19) is plotted as a function of wave number for three temperatures. The maxima occur at values of k corresponding to a phonon energy of $\sim 3k_B T$. Thus, the wavelength of the dominant phonons is roughly $2\pi\hbar c_0/3k_B T$ which at $P = 0$ is equal to $40/T$ Å. The

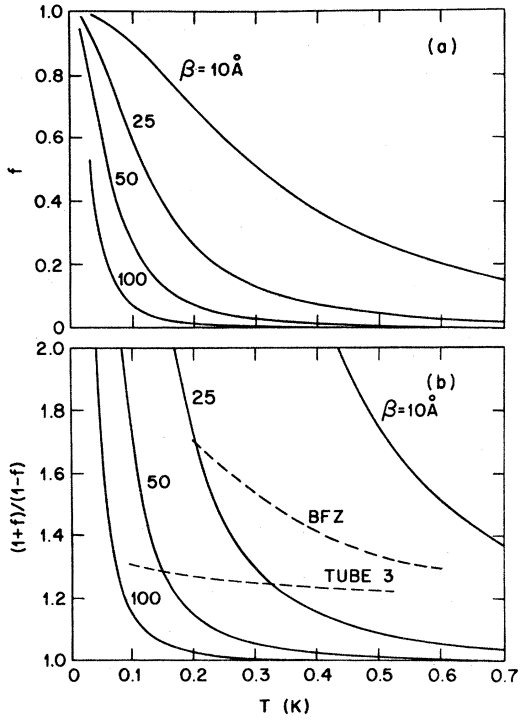

FIG. 11. The amount of specular reflection as a function of temperature. The solid curves correspond to uniformly rough surfaces and were computed for phonons in liquid helium at zero pressure using Eq. (19). The dashed curve labeled BFZ is the result obtained by Berman, Foster, and Ziman (Ref. 16) from thermal conductivity measurements on a sapphire crystal.

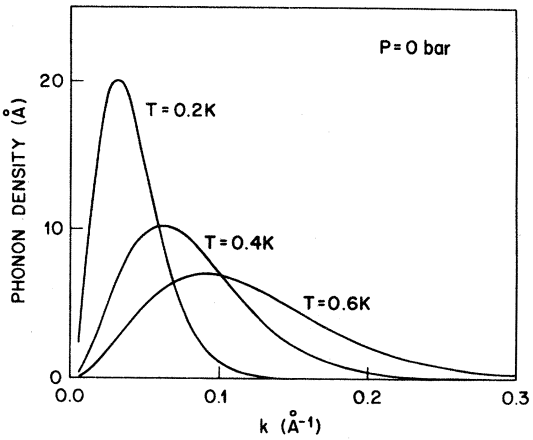

FIG. 12. The energy-weighted density of phonons for three temperatures. The curves have been normalized so that the area under each curve is unity. The maxima occur at values of k corresponding to a phonon energy of $\sim 3k_BT$.

curves plotted in Fig. 11 therefore show that when the dominant phonon wavelength becomes of the order of β, specular reflections are becoming significant. Thus if the effects of specular reflections are to be minimized, β must be considerably greater than $\lambda_{\text{dominant}}$. For measurements extending down in temperature to 0.1 K this means β must be much greater than about 400 Å. It is for this reason that we attempted to obtain a uniform surface roughness of $\sim 1-10$ μm (see Fig. 2) which is still small in comparison to our smallest tube diameter of about 1 mm. And indeed for tubes 1, 2, 4, and 5 there is no evidence of significant specular reflection: at low temperatures, where the effects of specular reflection should be largest, we find that, within our overall accuracy, the y data (Fig. 10) for each of the tubes tends approximately to 1. This is the result expected if the scattering at the wall is purely diffusive. We note also that since $\lambda_{\text{dominant}} \propto c_0$ the effect of specular reflection from a uniformly rough tube should be exaggerated at the higher pressures, but there is no appreciable pressure dependence to the zero temperature intercept.

The results for tube 3 are quite different. The y data for this tube are, at low temperature, approximately 25% greater than for the other tubes indicating that here there is specular reflection. The depth of the minimum is also greater for this tube which is consistent with the expectation that the amount of specular reflection increases with decreasing temperature. Moreover the increase in the depth of the minimum as the pressure is increased from 0.1 to 5 bar would be explained since the position of the minimum shifts to higher temperature. Estimated values of f, obtained by comparison with the results for the other tubes are plotted in Fig. 11. The temperature dependence of $(1+f)/(1-f)$ is radically different from the curves computed for a uniformly rough surface. But since this tube is unique among several tubes prepared in the same manner, there is no reason to expect that its surface is uniform. It is possible that some portion of the aluminum mandrel on which the nickel tube was plated was not throughly sand blasted, leaving small regions, not visually detectable, which were relatively smooth. Also plotted in Fig. 11 are results obtained by Berman, Foster, and Ziman[16] from their conductivity measurement on sapphire, and which agree more favorably with our findings, particularly if allowance is made for the much larger sound velocity in this crystal. These authors have explained their results as being due to a distribution of values of β. These arguments would also apply to our results. Apparently, the temperature dependence of f for any real surface can be determined only empirically, which further emphasizes the need for reducing the amount of specular reflection to a very small level if quantitative information is to be extracted from low-temperature thermal conductivity measurements. The results for

tube 3 will, therefore, not be included in the further analysis of the data.

E. Finite-tube-length corrections

In the Casimir regime, the thermal conductivity, while not depending on the spacing between the thermometers, does depend on the overall length L of the sample. This is a consequence of the phonons scattering from the ends of the tube. As was shown by Berman *et al.*[15] even for samples possessing perfectly rough walls ($f=0$) it is still necessary to apply corrections due to the finite length of the samples. For small values of d/L the results of their calculations are approximated if d in Casimir's relation [Eq. (1)] is replaced by $d(1-1.3d/L)$. Thus the thermal conductivities measured in tubes of finite length will be less than those computed using the unmodified Casimir equation. This means that the results plotted in Fig. 10 should tend, at low temperature, to y values that are somewhat less than unity. The values of L/d for all of the tubes can be determined from Table I. They imply that the length correction should range from about 5% for tube 1 to about 7% for tube 5. This may at least partially explain the trend of the data, with increasing tube diameter, towards smaller values of y at the minimum. It must be noted however that the length correction has been determined only in the Casimir regime. In the intermediate and viscous flow regions the effects of a finite tube length should be progressively reduced. In the absence of any appropriate theory, we have simply chosen to correct all of the y values for finite-tube-length effects by multiplying these data by the expression

$$F=1+1.3(d/L)e^{-d/\Lambda} \quad . \tag{20}$$

This function shows the proper behavior for the two extremes of d/Λ and implies that the correction is still significant in the region of the minimum ($d/\Lambda \approx 1$) in agreement with the experimental indications. Although any errors introduced by this procedure will affect our quantitative conclusions concerning the minimum in y, the consequences of using this particular interpolation function should be minimal in the viscous flow regime.

F. Slip coefficient

Equation (3) given in the Introduction implies that the expression for y is the viscous flow regime should be given by

$$y=\frac{5}{32}\frac{d}{\Lambda(T)}g(T) \quad . \tag{21}$$

Therefore a plot of the appropriate y data as a function of the tube diameter along isotherms should show a set of straight lines emanating from the origin. The data obtained at 0.1 and at 2 bar are plotted in this manner in Fig. 13 for several temperatures. The results are clearly consistent with a set of straight lines passing through a single y axis intercept, however, the intercept is considerably greater than zero. This can be explained as being due to the slip of the normal fluid at the boundary.

In obtaining Eq. (3), use was made of Poiseuille's formula

$$\dot{V}=\frac{\pi d^4}{128\eta}\frac{dp}{dx} \quad , \tag{22}$$

which relates the volume flow rate of a gas to the pressure gradient. This relation is based, however, on the assumption that the fluid velocity at the wall of the tube is zero. Actually the gas slips at the wall and moves with some velocity $v_{\text{wall}}=\zeta dv/dr$. Here r is the radial distance from the axis of the tube. The

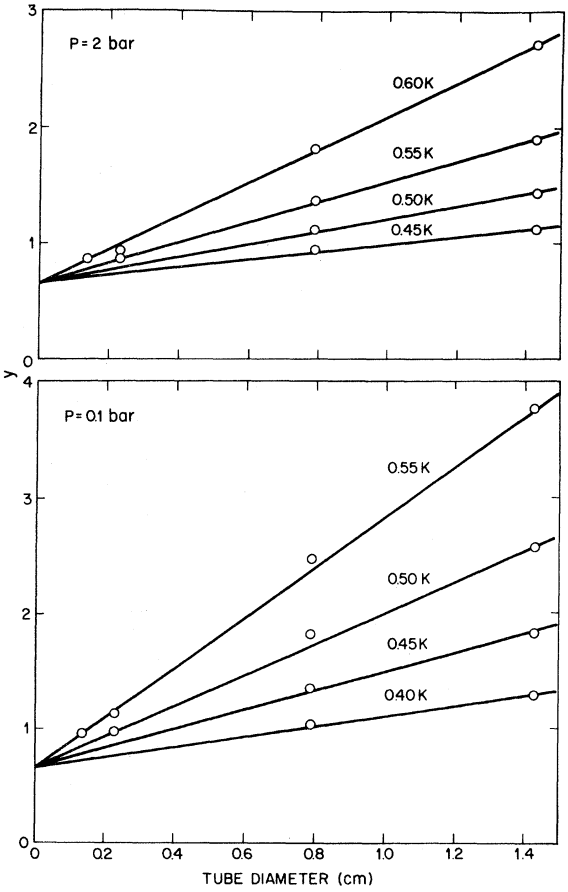

FIG. 13. The reduced conductivity y in the viscous flow regime plotted vs the tube diameter for several isotherms. The y-axis intercept is directly related to the slip coefficient.

parameter ζ, which has length units, is the slip coefficient. For ordinary gases both experiment and theory indicate[17] that ζ should be approximately equal to Λ, if the phonons scatter diffusively from the tube walls. With allowance for slip at the boundary, the Poiseuille equation becomes

$$\dot{V} = \frac{\pi d^4}{128\eta}\frac{dp}{dx}\left(1+8s\frac{\Lambda}{d}\right) , \tag{23}$$

where $s = \zeta/\Lambda$ is the reduced slip coefficient which is a constant of the order of unity. For the case of the phonon gas, the driving force is the gradient in fountain pressure given by

$$\frac{dp}{dx} = S\frac{dT}{dx} . \tag{24}$$

S is the entropy per unit volume. Equations (23) and (24) and the relation $\dot{Q} = TS\dot{V}$ then lead to the expression for the heat flow

$$\dot{Q} = \frac{\pi d^4 S^2 T}{128\eta}\frac{dT}{dx}\left(1+8s\frac{\Lambda}{d}\right) . \tag{25}$$

Using Eq. (2) to relate η and Λ and neglecting the effects of the rotons, which are small at low pressures, Eq. (25) implies that

$$\kappa = \tfrac{5}{32}\frac{d}{\Lambda}g\left(\tfrac{1}{3}C_{ph}\langle c_g\rangle d\right)\left(1+8s\frac{\Lambda}{d}\right) , \tag{26}$$

where g is defined by Eq. (4) and is a quantity which is approximately equal to one (see Fig. 9). It then follows that in the viscous flow regime

$$y = \tfrac{5}{32}\frac{d}{\Lambda}g + \tfrac{5}{4}sg . \tag{27}$$

Thus the y intercept in Fig. 13 quite directly gives the reduced slip coefficient.

The straight lines were actually drawn with an intercept at $y = \frac{2}{3}$ which corresponds to the value $s = \frac{8}{15}$ estimated by Whitworth following the method used by Millikan[18] for ordinary gases. Much more detailed calculations made recently by Benin and Maris[4] and by Jensen *et al.*[19] yield the slip coefficients 0.592 and 0.579, respectively. Using either of these two theoretical values, however, leads to a poorer fit of the experimental data.

It should be noted that several of the data points plotted in Fig. 13 have $y \approx 1$ and, therefore, are not in the well developed viscous flow regime. These y values should then lie above the corresponding straight lines, suggesting that the y intercept may actually be even somewhat less than $\frac{2}{3}$.

G. Roton effects

In addition to limiting the mean free path of the phonons (see Sec. III H), the rotons play a more direct role in determining the thermal conductivity of the liquid. An allowance must be made for the roton enhancement of the heat flow which becomes particularly significant at the higher temperatures and pressures considered.

At sufficiently high temperatures both the phonons and the rotons should have mean free paths that are small compared to the tube diameter. Thus, according to two-fluid hydrodynamics

$$S = S_r + S_{ph} .$$

There is also the relation[20]

$$\eta = \eta_r + \eta_{ph} .$$

But for $T \lesssim 0.7$ K, η_{ph} is large compared to η_r at all pressures and so $\eta \approx \eta_{ph}$. Thus, with the rotons taken into account, Eq. (27) becomes[2]

$$Y \equiv y\left(1+\frac{S_r}{S_{ph}}\right)^{-2} = \tfrac{5}{32}\frac{d}{\Lambda}g + \tfrac{5}{4}sg . \tag{28}$$

The quantity S_r/S_{ph} is plotted along several isobars in Fig. 14, which shows that even below 0.5 K the roton effects become large at high pressure.

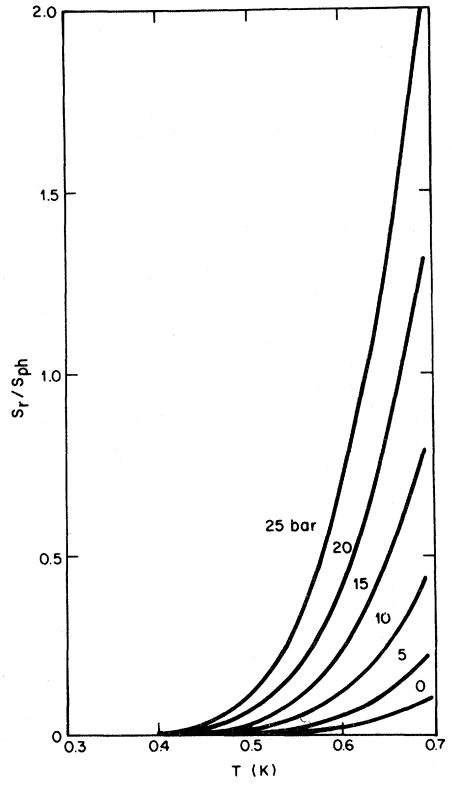

FIG. 14. Ratio of the roton and phonon entropies plotted vs the temperature.

As stated above, Eq. (28) is valid only if both the phonons and the rotons are in the hydrodynamic regime. Considering first the rotons: The expressions given by Landau and Khalatnikov[20] lead to the roton mean free path (in cm) being approximately given by $2\times10^{-8}\rho^{5/3}e^{\Delta/k_BT}$. The implication is that this mean free path should be small compared to the tube diameters at all pressures for temperatures beyond the minima. Also, at high pressures the experimental observation of roton second sound[21] is a direct indication that here the rotons are hydrodynamic. Evidence that the phonons are at least approaching this regime at the higher temperatures and at all pressures, is the fact that each of the strings of y data presented in Fig. 10 shows a minimum of about the same depth. This means then, that even at 25-bar pressure, where the roton effects are greatest, the minimum in the corrected data (at which $\Lambda\approx d$) cannot occur at a temperature which is much greater than the position of the minimum in y. Consequently, we expect that the phonons should also be hydrodynamic for large values of y, at least at the lower pressures.

H. Phonon mean free path

The mean free path of the phonons can be extracted from the conductivity data in the viscous flow regime using Eq. (28) which with $s=\frac{8}{15}$ can be rewritten

$$\Lambda=\tfrac{5}{32}d/(Y/g-\tfrac{2}{3}) \ . \tag{29}$$

This form of the expression emphasizes the fact that for small values of Y, Λ is quite sensitive to the exact choice for the slip coefficient and also to possible systematic errors in Y. Consequently, the most reliable results for Λ should be obtained using the measurements on the largest diameter tubes. Values of Λ vs T at 0.1 bar are plotted in Fig. 15 for tubes 4 and 5. The Y data were corrected for finite tube length effects and were normalized so that they agreed at the minimum value of Y. The data over most of the temperature range plotted fall quite accurately on a straight line in this log-log plot which corresponds approximately to a T^{-5} temperature dependence. The systematic deviations from this behavior at the low-temperature end are for data outside of the various flow regime where Eq. (29) is no longer valid. Near 0.4 K the two strings of data merge which indicates that when $\Lambda\approx\frac{1}{2}d$ the thermal conductivity is already that characterizing viscous flow of the phonons. This implies that the Λ results for tube 5 should be valid for $\Lambda\lesssim0.7$ cm or equivalently for $T\gtrsim0.35$ K. At lower temperatures the position of the minimum in Y, can be used to determine values of Λ since the minimum occurs when $\Lambda\approx1.53d$ (Sec. III I). The

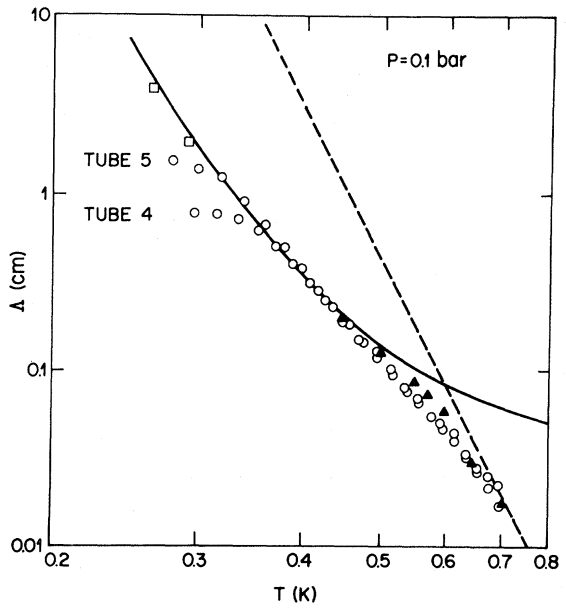

FIG. 15. Temperature dependence of the phonon mean free path at $P=0.1$ bar. The circles at the lowest temperatures were determined using data outside of the viscous flow regime and, therefore, do not correspond to the intrinsic values of Λ. The squares were determined using the positions of the Knudsen minima for tubes 4 and 5. The solid triangles are Whitworth's measurements (Ref. 2). The dashed line is proportional to T^{-9} and is the mean free path for four phonon processes calculated by Landau and Khalatnikov (Ref. 20). The solid curve was calculated according to Maris's model (Refs. 23 and 24) using the parametrization of the phonon dispersion relation given by Eq. (31).

data obtained for tubes 4 and 5 using this relation are plotted as open squares and are consistent with the mean-free-path results for $\Lambda\lesssim0.7$ cm. The measurements of Whitworth[2] at $P=0$, solid triangles, are also shown in the figure. His results have actually been scaled by $\frac{5}{3}$ to account for the different expression he used to relate η and Λ. There is good agreement, especially for the two pairs of points on the extremes of his temperature range.

The dashed line in Fig. 15 corresponds to the expression (in cgs units)

$$\Lambda=4.50\times10^{-48}\frac{\rho^2c_0^{11}}{(u+1)^4}T^{-9} \ , \tag{30}$$

which was derived by Landau and Khalatnikov[20] assuming that the phonon dispersion relation was normal and thus that three phonon processes ($3pp$) were not allowed.[22] In this expression ρ is the density and u is the Grüneisen parameter $(\rho/c_0)(dc_0/d\rho)$. As first shown by Whitworth, this expression is clearly inconsistent with the experimental results. It is now known, however, that the phonon dispersion is anomalous and that three-phonon small-angle

processes can take place.[22] Assuming that this is the dominant scattering mechanism Maris[23] calculated the normal fluid viscosity. His results were based on a phonon dispersion curve which was very similar to that plotted in Fig. 7 and agreed well with the Whitworth data between 0.45 and 0.6 K. Almost identical theoretical results were obtained by Benin[24] using a simplified method. The present data indicate however that the temperature dependence of Λ in this temperature range is somewhat steeper than found by Whitworth. In addition the new data extend to lower temperatures and can thus provide a more severe test of the theory. The solid curve in the figure has been determined by numerally evaluating Benin's expression [his Eq. (12)] using the dispersion relation

$$\epsilon = c_0 \hbar k (1 - \alpha_2 k^2 - \alpha_4 k^4) \ , \tag{31}$$

with $\alpha_2 = -1.1$ Å^2 and $\alpha_4 = 8.2$ Å^4. This curve provides an excellent description of the data with $T \lesssim 0.5$ K. However, since there is a strong correlation between α_2 and α_4 fits which are nearly as good can be obtained with other values of these parameters as can be inferred from the curves plotted in Fig. 16. In Fig. 15 the discrepancy between the theoretical curve and the experimental data at the higher temperatures can be explained as being largely due to the unrealistic shape of the dispersion curve described by Eq. (31) near the maximum in the sound velocity. As a consequence, the cutoff in the integration of Benin's expression occurs at too low a wave vector.

Presumably a more flexible function describing the phonon dispersion relation could be used to more accurately fit the mean-free-path results over the complete temperature range. The possibility of accurately determining α_2 would be improved considerably if the experimental data extended down to much lower temperatures since Benin's relation implies that Λ should tend toward a T^{-9} temperatures dependence with an amplitude easily related to α_2. It should also be noted that there is some ambiguity in the highest temperature results since higher-order scattering processes may become important as discussed below.

As the pressure is increased to 2 bar the position of the minimum in y (Fig. 10) shifts to higher temperatures which implies an increase in the mean free path. In Maris's model this is explained in part as being due to a phonon dispersion which deviates less from linear behavior leading to three phonon processes which are more nearly colinear. Thus more of these small-angle collisions are needed to make up a large-angle collision. The Λ results at 2 bar are plotted in Fig. 17. Below approximately 0.6 K the results are as expected. At higher temperatures, however, the temperature dependence of Λ becomes steeper, which is evidence that other scattering processes are becoming significant. The Λ data at 5 and 10 bar are also plotted in Fig. 17 and exhibit a temperature dependence for $T \gtrsim 0.6$ K which is even greater than the T^{-9} dependence expected for four phonon processes. This would suggest that phonon-roton scattering may be important at these higher pressures.

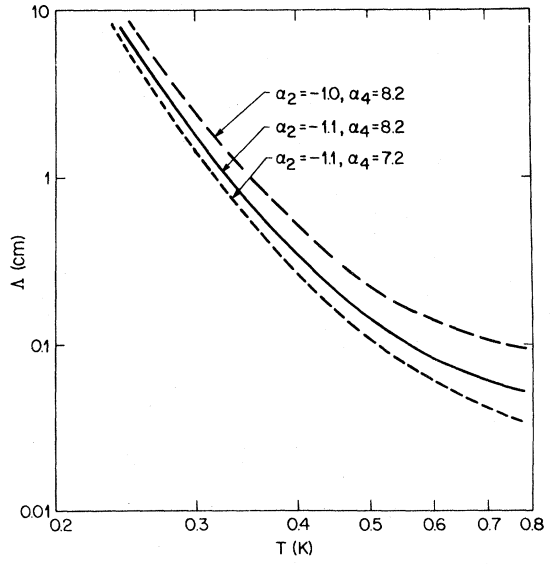

FIG. 16. Benin's expression (Ref. 24) for Λ evaluated using the dispersion relation given by Eq. (31).

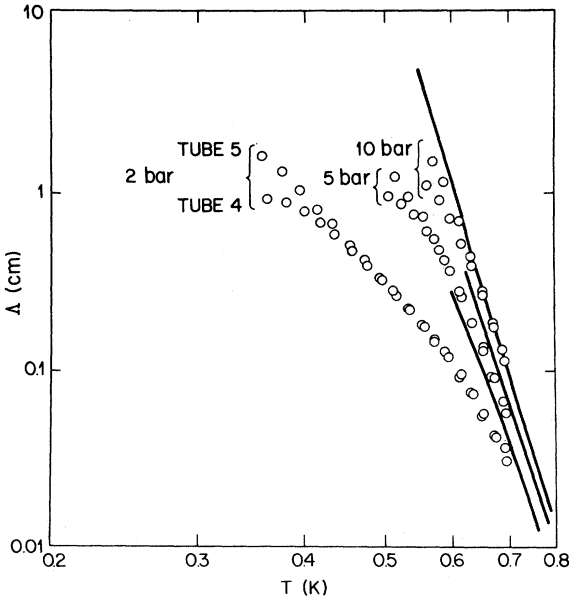

FIG. 17. Mean-free-path results at sample pressures of 2, 5, and 10 bar. The solid curves correspond to $3\Lambda_{LK}$.

The Landau-Khalatnikov (LK)[20] expression for the phonon mean free path, which takes into account only the four phonon processes and phonon-roton scattering (and which involves no adjustable parameters) can be written

$$\frac{1}{\Lambda_{LK}} = \frac{2.90\times10^{32}}{c_0^6\rho^{4/3}} T^{9/2} e^{-\Delta/k_B T} \times \left[0.133 + 13.3\times10^{11}\frac{\rho^{10/3}}{c_0^2}\right] + 2.22\times10^{47}\frac{(u+1)^4}{\rho^2 c_0^{11}} T^9 \ . \quad (32)$$

Numerical values for $\hbar$, etc., have been substituted and the empirical relations[7,25,26] (in cgs units)

$$p_0 = 3.859\times10^{-19}\rho^{1/3}$$

and

$$\left(\frac{\mu}{m_4}\right)^{1/2}\left(\frac{p_0}{\hbar}\right)^2 = 1.49\times10^{16} \quad (33)$$

have been used. In the above equation Δ, p_0, and μ are the usual roton parameters. Λ_{LK} is plotted as a function of T along several isobars in Fig. 18, using values of c_0, u, and ρ from Ref. 27 and values of Δ from Ref. 7. These curves qualitatively show the same temperature and pressure dependence as the higher temperature experimental results shown in Fig. 17, however, the magnitude of Λ_{LK} is a factor of 3 too small. The solid curves plotted in Fig. 17 correspond to 3 Λ_{LK}. Note that although we compare and find agreement with the scaled form of Eq. (32), the Landau-Khalatnikov result for the four phonon process should hold only if the phonon dispersion is normal.

The experimental results for Λ at pressures greater than 10 bar are unreliable and have not been included in Fig. 17. The large uncertainty in the data arises mainly from the fact that the roton correction (Sec. III G) increases rapidly with increasing pressure. However, these data can be checked for consistency with the findings at lower pressures. In Fig. 19 the quantity $y/(\frac{5}{32}dg/\Lambda + \frac{5}{4}sg)$ is plotted versus T at $P = 20$ bar using $\Lambda = 3\ \Lambda_{LK}$. In agreement with Eq. (28), the solid curve in the figure corresponding to $(1+S_r/S_{ph})^2$ describes these data well.

Making the assumption that

$$\frac{1}{\Lambda} \approx \frac{1}{\Lambda_{3pp}} + \frac{1}{3\Lambda_{LK}} \quad (34)$$

values of Λ_{3pp} have been extracted from the data at 0.1 and at 2 bar and are shown in Fig. 20. The smooth curves drawn through the data correspond to the expressions

$$\Lambda_{3pp}(0.1) = 2.13\times10^{-5}T^{-9} + 6.34\times10^{-3}T^{-4}$$

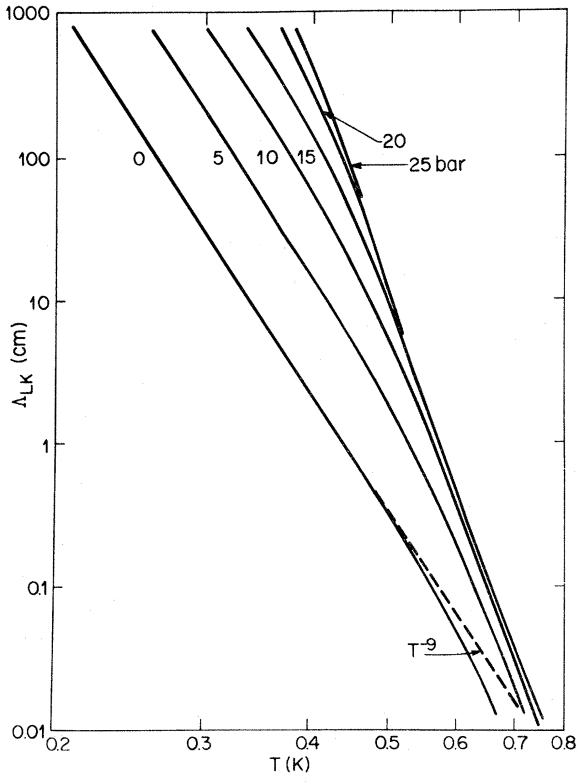

FIG. 18. Λ_{LK} determined using Eq. (32).

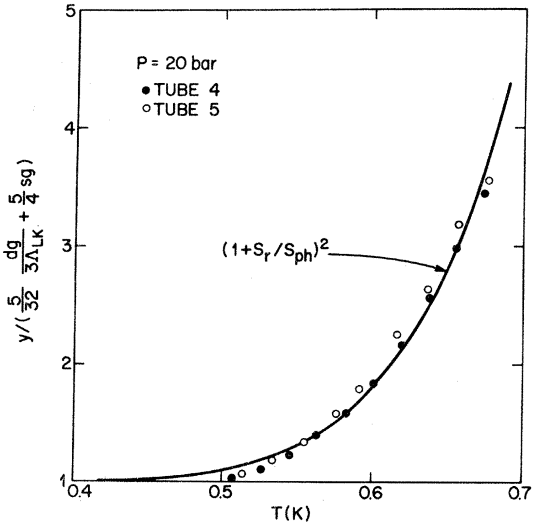

FIG. 19. Comparison of the quantities $y/(\frac{5}{32}dg/3\Lambda_{LK} + \frac{5}{4}sg)$ and $(1+S_r/S_{ph})^2$ at $P = 20$ bar. The good agreement is in accord with Eq. (28) and the results for Λ at lower pressures.

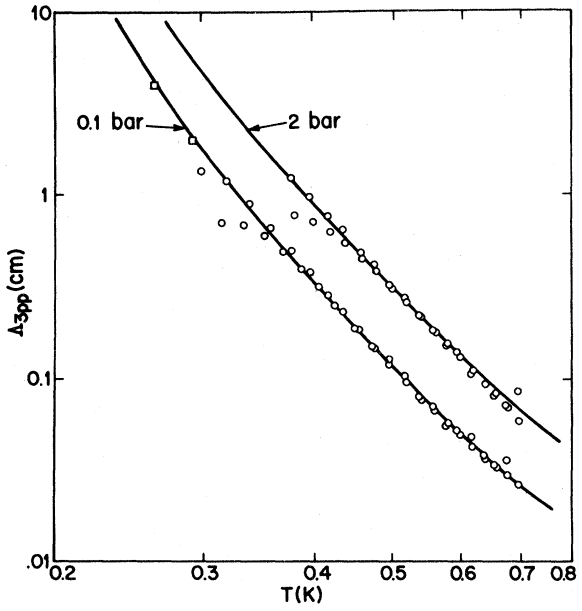

FIG. 20. Λ_{3pp} extracted from the experimental data using Eqs. (29) and (34). The solid curves correspond to Eq. (35).

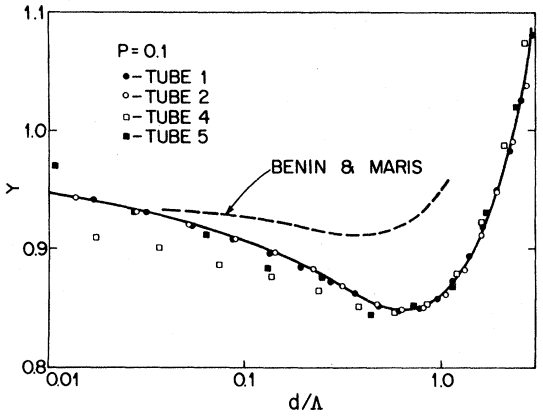

FIG. 21. Y vs d/Λ in the region of the minimum. Y reaches a minimum value of about 0.85 near $d/\Lambda = 0.65$. The dashed curve is due to Benin and Maris (Ref. 4). The solid curve is a smooth curve drawn through the data.

and

$$\Lambda_{3pp}(2) = 2.6\Lambda_{3pp}(0.1) \ . \tag{35}$$

I. Knudsen minimum

In the viscous flow regime Y can be written as a function of d/Λ [Eq. (28)]. At lower temperatures, in the region of the minimum, one would expect this ratio to continue to be the relevant parameter. Thus in Fig. 21, Y at $P = 0.1$ bar has been plotted versus d/Λ for tubes 1, 2, 4, and 5 using values of Λ determined by Eqs. (34) and (35). These Y values are the y data shown in Fig. 10 corrected for finite tube length and roton effects, i.e.,

$$Y = y[1 + 1.3(d/L)e^{-d/\Lambda}](1 + S_r/S_{ph})^{-2} \ . \tag{36}$$

Y thus corresponds to the y values that would have been measured in an infinitely long tube if only phonons were present. Additional scaling factors of 0.995, 1.04, and 1.05 were applied, respectively, to the results for tubes 2, 4, and 5 to improve the agreement. The magnitude of these overall scaling factors is consistent with the estimates of the possible systematic errors in the measurements. With the exception of the results for tube 4 below the minimum, all of the values plotted fall quite accurately on the universal curve smoothly drawn through the data points. There is no obvious explanation for the departures of the tube 4 results. The higher-pressure data should also fall on this curve, however, the uncertainities increase rapidly with increasing pressure. This is due to the increasing importance of the roton corrections to y which near the minimum cannot be assumed to be the simple factor given in Eq. (36). There is also then the consequential problem that the position of the y minima cannot be used to extend the data for Λ down to lower temperatures. Moreover, Λ develops a strong temperature dependence at the higher pressures which leads to larger uncertainties in $\Lambda(T)$.

The results plotted in Fig. 21 indicate that Y reaches a minimum value of about 0.85 when $d/\Lambda \approx 0.65$. Whitworth[2] also found the minimum to have about the same depth, however he places the minimum[28] at $d/\Lambda = 0.87 \pm 0.13$. This discrepancy may be in part due to the fact that all of Whitworth's data showed evidence of specular reflection for which a correction had to be applied. There is also some uncertainty in his temperature scale. The dashed curve in Fig. 21 shows the recent theoretical results of Benin and Maris.[4] Their curve exhibits a minimum y value of 0.91 at $d/\Lambda = 0.40$.

ACKNOWLEDGMENTS

I would like to thank G. Ahlers, R. N. Bhatt, and H. J. Maris for many helpful discussions. I am also grateful to P. Busch, who contributed greatly to all technical aspects of this work.

[1]H. B. Casimir, Physica (Utrecht) 5, 495 (1938).
[2]R. W. Whitworth, Proc. R. Soc. London Ser. A 246, 390 (1958).
[3]S. Simons, Proc. R. Soc. London Ser. A 315, 239 (1970).
[4]D. Benin and H. J. Maris, Phys. Rev. B 18, 3112 (1978).
[5]P. R. Roach, J. B. Ketterson, and M. Kuchnir, Rev. Sci. Instrum. 43, 898 (1972).
[6]D. S. Greywall and P. A. Busch, Rev. Sci. Instrum. 51, 509 (1980).
[7](a) D. S. Greywall, Phys. Rev. B 18, 2127 (1978); (b) 21, 1329(E) (1980).
[8]G. Ahlers, Phys. Rev. 171, 275 (1968); see also K. H. Mueller, G. Ahlers, and F. Pobell, Phys. Rev. B 14, 2096 (1976).
[9]A. C. Anderson, J. H. Anderson, and M. P. Zaitlin, Rev. Sci. Instrum. 47, 407 (1976).
[10]R. Berman, *Thermal Conduction in Solids* (Clarendon, Oxford, 1976).
[11]C. Boghosian and H. Meyer, Phys. Rev. 152, 200 (1966).
[12]R. J. Donnelly, J. A. Donnelly, and R. N. Hills (unpublished).
[13]W. G. Stirling, J. R. D. Copley, and P. A. Hilton, in proceedings of an IAEA symposium, *Neutron Inelastic Scattering, 1977* (IAEA, Vienna, 1978), Vol. II, p. 45.
[14]R. C. Dynes and V. Narayanamurti, Phys. Rev. B 12, 1720 (1975).
[15]R. Berman, F. E. Simon, and J. M. Ziman, Proc. R. Soc. London Ser. A 220, 171 (1953).
[16]R. Berman, E. L. Foster, and J. M. Ziman, Proc. R. Soc. London Ser. A 231, 130 (1955).
[17]E. H. Kennard, *Kinetic Theory of Gases* (McGraw-Hill, New York, 1938).
[18]R. A. Millikan, Phys. Rev. 21, 217 (1923).
[19]H. Højgaard Jensen, H. Smith, P. Wölfle, K. Nagai, and T. M. Bisgaard (unpublished).
[20]L. D. Landau and I. M. Khalatnikov, Zh. Eksp. Teor. Fiz 19, 637 (1949); 19, 709 (1949).
[21]R. C. Dynes, V. Narayanamurti, and K. Andres, Phys. Rev. Lett. 30, 1129 (1973).
[22]H. J. Maris, Rev. Mod. Phys. 49, 341 (1977).
[23]H. J. Maris, Phys. Rev. A 8, 1980 (1973).
[24]D. Benin, Phys. Rev. B 11, 145 (1975).
[25]O. W. Dietrich, E. H. Graf, C. H. Huang, and L. Passell, Phys. Rev. A 5, 1377 (1972).
[26]A. D. B. Woods, P. A. Hilton, R. Scherm, and W. G. Stirling, J. Phys. C 10, L45 (1977).
[27]B. M. Abraham, Y. Eckstein, J. B. Ketterson, M. Kuchnir, and P. R. Roach, Phys. Rev. A 1, 250 (1970).
[28]This value differs from that given in Whitworth's paper by a factor of $\frac{3}{5}$. This is due to the different expressions used to relate η and Λ.

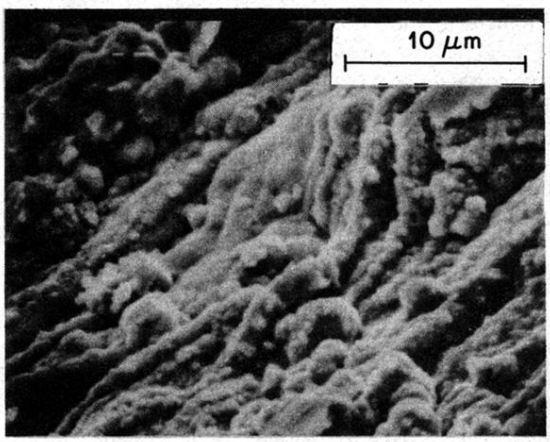

FIG. 2. Inside surface of the sample containment tubes.